PHYSICAL REVIEW B **94**, 201410(R) (2016)

Relativistic k · p Hamiltonians for centrosymmetric topological insulators from *ab initio* wave functions

I. A. Nechaev[1,2,3] and E. E. Krasovskii[4,5,6]

[1]*Centro de Física de Materiales CFM–MPC and Centro Mixto CSIC-UPV/EHU, 20018 San Sebastián/Donostia, Spain*

[2]*Tomsk State University, 634050 Tomsk, Russia*

[3]*Saint Petersburg State University, 198504 Saint Petersburg, Russia*

[4]*Departamento de Física de Materiales UPV/EHU, Facultad de Ciencias Químicas, UPV/EHU, Apartado 1072, 20080 San Sebastián/Donostia, Spain*

[5]*Donostia International Physics Center, 20018 San Sebastián/Donostia, Spain*

[6]*IKERBASQUE, Basque Foundation for Science, 48013 Bilbao, Spain*

(Received 13 July 2016; revised manuscript received 14 November 2016; published 28 November 2016)

We present a method to microscopically derive a small-size **k** · **p** Hamiltonian in a Hilbert space spanned by physically chosen *ab initio* spinor wave functions. Without imposing any complementary symmetry constraints, our formalism equally treats three- and two-dimensional systems and simultaneously yields the Hamiltonian parameters and the true $\mathbb{Z}_2$ topological invariant. We consider bulk crystals and thin films of Bi_2Se_3, Bi_2Te_3, and Sb_2Te_3. It turns out that the effective continuous **k** · **p** models with open boundary conditions often incorrectly predict the topological character of thin films.

DOI: 10.1103/PhysRevB.94.201410

The electronic structure of topological insulators (TIs) has been the focus of theoretical research regarding linear response, transport properties, Hall conductance, and the motion of Dirac fermions in external fields [1,2]. These problems call for a physically justified model Hamiltonian of small dimension. As in semiconductors, it is thought to be sufficient that the model accurately reproduces the TI band structure near the inverted band gap [3]. The desired Hamiltonian is derived either from the theory of invariants [4] or within the **k** · **p** perturbation theory using the symmetry properties of the basis states [5].

In Ref. [3], along with the pioneering prediction of the topological nature of Bi_2Se_3, Bi_2Te_3, and Sb_2Te_3, a four-band Hamiltonian was first constructed from the theory of invariants, which is presently widely used to analyze the properties of bulk TIs as well as their surfaces and thin films [6–14]. The Hamiltonian parameters in Ref. [3] were obtained by fitting *ab initio* band dispersion curves. Later, an attempt was made [15] to recover the Hamiltonian of Ref. [3] by a **k** · **p** perturbation theory with symmetry arguments and to derive its parameters from the *ab initio* wave functions of the *bulk* crystals. Furthermore, in Ref. [15] the effective Landé g factors for the Zeeman splitting [4,5] were introduced within the **k** · **p** theory of TIs.

To analyze how the properties of *thin films* are inherited from the bulk TI features, effective continuous models have been developed: They are based on the substitution $k_z \to -i\,\partial_z$ (originally introduced for slowly varying perturbations [16]) in the Hamiltonian of Ref. [3] and on the imposition of the open boundary conditions [15,17–19]. These models predict a variety of intriguing phenomena at the surfaces, interfaces, and thin films of TIs [20–23]. A fundamental issue here is the topological phase transition between an ordinary two-dimensional (2D) insulator and a quantum spin Hall insulator (QSHI). Apart from the theoretical prediction, the model parameters are fitted to the measured band dispersion to deduce the topological phase from the experiment [24,25]. By analyzing the signs and relative values of the parameters of the empirically obtained effective model, a judgment is made on whether the edge states would exist in a given TI film, the logic being similar to that of Ref. [26]: The valence band should have a positive and conduction band a negative effective mass.

In order to avoid any ambiguity in deriving the model Hamiltonian and to treat three-dimensional (3D) and 2D systems within the same formalism, one needs an *ab initio* and internally consistent scheme that realizes the **k** · **p** theory with the full inclusion of the microscopic structure of the system and generates a compact and physically transparent form of the Hamiltonian of a given size. A few attempts have been recently undertaken to predictably construct model Hamiltonians for classical bulk semiconductors [27] and graphene-based systems [28].

In this Rapid Communication, we report a method to *microscopically* derive the relativistic Hamiltonian $H_{\mathbf{kp}}$ accurate up to the second order in **k** from the spinor wave functions obtained with the all-electron full-potential extended linearized augmented plane wave method (ELAPW). The size of $H_{\mathbf{kp}}$ is determined by the dimension of the subspace spanned by the physically chosen basis states. The form of the Hamiltonian is dictated by the symmetry of the wave functions unitary transformed to diagonalize the z component of the total angular momentum and by a universal prescription to choose their phases. Here, we apply this approach to centrosymmetric bulk crystals as well as to thin films of Bi_2Se_3, Bi_2Te_3, and Sb_2Te_3 up to six quintuple layers (QLs). For each film, we calculate the topological invariant, indicating whether it is a QSHI. We conclude on the validity of the topological analysis based on the effective models (including the *ab initio* derived ones) by comparing the predictions made by the **k** · **p** Hamiltonian with the actual properties of the film. Furthermore, within our approach, we derive the **k** · **p** Zeeman term for the films.

We construct the model Hamiltonian as a second-order **k** · **p** expansion around the point $\mathbf{k} = \mathbf{0}$. To avoid any ambiguity, we obtain the expansion coefficients directly from *ab initio*

eigenfunctions at Γ. For systems with inversion symmetry, the energy bands E_n are doubly degenerate with two orthogonal wave functions Ψ_{n1} and Ψ_{n2} that are parity eigenfunctions at the time reversal invariant momenta (TRIM). The $\mathbf{k}\cdot\mathbf{p}$ Hamiltonian is represented in the basis of these functions in terms of the matrix elements $\langle\Psi_{ni}|\boldsymbol{\pi}|\Psi_{mj}\rangle$ of the velocity operator $\boldsymbol{\pi} = -i\hbar\nabla + \hbar[\boldsymbol{\sigma}\times\nabla V]/4m_0c^2$ [29]. Here, $\boldsymbol{\sigma}$ is the vector of Pauli matrices and $V(\mathbf{r})$ is the crystal potential. In the $\mathbf{k}\cdot\mathbf{p}$ expansion, $H_{\mathbf{kp}} = H^{(0)} + H^{(1)} + H^{(2)}$, the zero-order term is just the band energy, $H^{(0)}_{nimj} = E_n\delta_{mn}\delta_{ij}$, the linear term is $H^{(1)}_{nimj} = (\hbar/m_0)\mathbf{k}\cdot\boldsymbol{\pi}_{nimj}$, and the second-order term is

$$H^{(2)}_{nimj} = \frac{\hbar^2k^2}{2m_0}\delta_{mn}\delta_{ij} + \frac{\hbar^2}{m_0^2}\sum_{\alpha\beta}k_\alpha D^{\alpha\beta}_{nimj}k_\beta,$$

where $\alpha,\beta = x,y,z$, and

$$D^{\alpha\beta}_{nimj} = \frac{1}{2}\sum_{n'i'}\pi^{\alpha}_{nin'i'}\pi^{\beta}_{n'i'mj}\left(\frac{1}{E_n - E_{n'}} + \frac{1}{E_m - E_{n'}}\right)$$

(see Refs. [4,5]). Here, m and n number the degenerate Kramers pairs, and i and j number the members of a pair. The index n' runs over all the bands excluding those forming the $\mathbf{k}\cdot\mathbf{p}$ basis (Löwdin's partitioning). Thus, when the dimension of $H_{\mathbf{kp}}$ equals the dimension of the original full Hamiltonian, the second-order term $H^{(2)}$ vanishes [30] (hereafter, we refer to this case as the full-size $\mathbf{k}\cdot\mathbf{p}$ calculation).

The *ab initio* band structure was obtained with the ELAPW method [31] using the full potential scheme of Ref. [32] within the local density approximation (LDA). The spin-orbit interaction is treated by a second variation method [33] including the scalar-relativistic bands up to at least 300 eV. This ensures a good convergence of the inverse effective mass, with a deviation from the second derivative of the $E(\mathbf{k})$ curves within 3%. The experimental crystal lattice parameters were taken from Ref. [35] with the LDA relaxed atomic positions of Refs. [36–38]. Figure 1 compares the *ab initio* bands with those obtained by diagonalizing our $\mathbf{k}\cdot\mathbf{p}$ Hamiltonians of small size (four- and eight-band) and of full size. Note that the full-size $\mathbf{k}\cdot\mathbf{p}$ calculation highly accurately reproduces the true bands: The error grows as k^2 [39], and at the Brillouin zone (BZ) boundary it is within 150 meV.

For each Kramers-degenerate level n, the spinor wave functions Ψ_{ni} form a two-dimensional basis. Numerically obtained functions are arbitrarily ordered and have unphysical phases, which, however, affect the structure of $H_{\mathbf{kp}}$ nondiagonal terms. In order to keep the same physically motivated ordering and to align the phases in different calculations, we first transfer to the basis that diagonalizes the z component of the total angular momentum $\mathbf{J} = \mathbf{L} + \mathbf{S}$ in the atomic sphere that has the largest weight in the nth band (see Figs. S5– S7 in the Supplemental Material (SM) [34]). This establishes the numeration of the wave functions $\Psi_{n1(2)} \to \Psi_{n\uparrow(\downarrow)}$. Next, we choose the phases of the new basis functions such that they become explicitly Kramers conjugate, $\Psi_{n\downarrow} = \hat{T}\Psi_{n\uparrow}$, where $\hat{T} = Ki\sigma_y$ is the time reversal operator and K is the complex conjugation operator. Finally, for two pairs of different parity, nth and mth, we turn the phases such that $i\pi^{x(z)}_{n\uparrow m\downarrow}$ be real.

For the bulk TIs we choose the basis of four states $\Psi_{v\uparrow},\Psi_{v\downarrow},\Psi_{c\uparrow},\Psi_{c\downarrow}$, where v and c stand for the valence and conduction band, respectively. This leads to the Hamiltonian [40]

$$H_{\mathbf{kp}} = C\tau_0\sigma_0 + M\tau_z\sigma_0 - V_\parallel\tau_x(\sigma_xk_y - \sigma_yk_x) - V_z\tau_y\sigma_0k_z, \quad (1)$$

with $C = C_0 + C_zk_z^2 + C_\parallel k_\parallel^2$, $M = M_0 + M_zk_z^2 + M_\parallel k_\parallel^2$, and $k_\parallel^2 = k_x^2 + k_y^2$. The 3D TI Hamiltonian (1) is the same (to within a unitary transformation) as in Refs. [3,15,17–19] (the explicit matrix form is presented by Eq. (S1) in the SM [34]). The Pauli matrix $\boldsymbol{\tau}$ operates in valence-conduction band space, whereas $\boldsymbol{\sigma}$ refers to the total angular momentum $\mathbf{J}$. In Eq. (1) a direct product of these matrices is implied.

For the bulk crystals, the parameters in Eq. (1) are listed in Table I, and the eigenvalues $E(\mathbf{k})$ of the resulting four-band Hamiltonian are shown in Figs. 1(a)–1(c) by red lines with solid circles. Note that already this minimal dimension of $H_{\mathbf{kp}}$ produces an absolute gap in the spectrum, and for Bi_2Se_3 and Sb_2Te_3 its width is very close to that obtained with the much more accurate eight-band Hamiltonian [see Eq. (S3) in the SM and blue lines with open rhombuses in

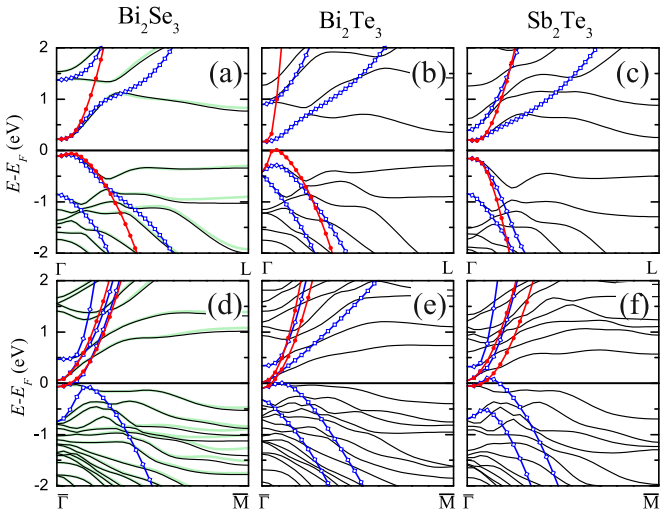

FIG. 1. Band structure (black lines) of (a)–(c) the bulk crystals and (d)–(f) 2QL films of Bi_2Se_3, Bi_2Te_3, and Sb_2Te_3 compared with the four-band (red lines with solid circles) and eight-band (blue lines with open rhombuses) $\mathbf{k}\cdot\mathbf{p}$ model. Results by the full-size Hamiltonian are shown by green lines for Bi_2Se_3. See also Figs. S1–S4 in the SM [34].

TABLE I. Parameters of the four-band $\mathbf{k}\cdot\mathbf{p}$ Hamiltonian (1) for the bulk TIs. We use Rydberg atomic units: $\hbar = 2m_0 = e^2/2 = 1$.

	Bi_2Se_3	Bi_2Te_3	Sb_2Te_3
$V_\parallel$ (a.u.)	0.349	0.556	0.513
V_z (a.u.)	0.255	0.125	0.163
C_0 (eV)	0.048	−0.123	0.023
C_z (a.u.)	0.37	0.70	−3.73
$C_\parallel$ (a.u.)	3.65	40.54	−1.83
M_0 (eV)	−0.169	−0.296	−0.182
M_z (a.u.)	0.88	2.43	5.81
$M_\parallel$ (a.u.)	7.71	46.55	13.47

Figs. 1(a)–1(c)]. An important point about the parameters of the Hamiltonian (1) is that they are very sensitive to details of the crystal geometry, as is the *ab initio* band structure [36–38]: Even a small variation in atomic positions leads to considerable changes of the parameters (see Table S1 in the SM [34]). Furthermore, in all the 3D systems considered (see Table I), the parameters of $H_{\mathbf{kp}}$ turned out to meet the conditions of the existence of the topological surface states [18]: The diagonal dispersion term $M_{z(\|)}$ is positive and is larger than the electron-hole asymmetry, $M_{z(\|)} > |C_{z(\|)}|$, although C_z and $C_\|$ are not negligible contrary to the assumption in Ref. [12]. Thus, our *ab initio* $\mathbf{k}\cdot\mathbf{p}$ Hamiltonian correctly predicts the topological character of these crystals in accord with the $\mathbb{Z}_2$ topological invariant ν_{3D} obtained from the parities of the wave functions at the TRIM points [41].

We now use our second-order perturbation theory to calculate the effective g factors entering the Zeeman term (see Eq. (S2) in the SM [34]) that appears in the presence of a static magnetic field [4,5],

$$g_z^{v(c)} = \frac{2}{im_0}\left(D^{xy}_{v(c)\uparrow v(c)\uparrow} - D^{yx}_{v(c)\uparrow v(c)\uparrow}\right),$$

$$g_\|^{v(c)} = \frac{2}{im_0}\left(D^{yz}_{v(c)\uparrow v(c)\downarrow} - D^{zy}_{v(c)\uparrow v(c)\downarrow}\right).$$

The most important is that the calculated values are one or even two orders of magnitude larger than the free-electron g factor, $g_0 \approx 2$. (The values obtained with the four-band $\mathbf{k}\cdot\mathbf{p}$ method are listed in Table S1 of the SM [34] for all the 3D TIs studied.) This result accords with the recent spin resonance measurements of the effective g factor in Bi_2Se_3 [42]: For the magnetic field parallel to the c axis, the experimental g_z factors are 27.30 ± 0.15 for electrons and 29.90 ± 0.09 for holes, while for the field perpendicular to the c axis the $g_\|$ factors are 19.48 ± 0.07 and 18.96 ± 0.04 for electrons and holes, respectively. In order to compare our theoretical effective-mass contributions to the g factors with the experiment, we should restrict to a two-band Hamiltonian in the basis $\Psi_{v(c)\uparrow}, \Psi_{v(c)\downarrow}$. For Bi_2Se_3, the two-band results are in good qualitative agreement with the experiment: Our g_z values are 11.6 (17.7) for electrons and 19.3 (42.4) for holes. For $g_\|$ we get 10.4 (16.1) and 12.1 (16.5) for electrons and holes, respectively. Here, the values obtained with the LDA-relaxed atomic positions are followed (in brackets) by those with experimental atomic positions.

In contrast to the bulk TIs, for finite-thickness TI films an ambiguous behavior is observed. For a 2D system, in the basis $\Psi^{\text{slab}}_{v\uparrow}, \Psi^{\text{slab}}_{c\downarrow}, \Psi^{\text{slab}}_{c\uparrow}, \Psi^{\text{slab}}_{v\downarrow}$, our $\mathbf{k}\cdot\mathbf{p}$ Hamiltonian reads (cf. Refs. [26,43])

$$H^{\text{slab}}_{\mathbf{kp}} = C\tau_0\sigma_0 + M\tau_z\sigma_z - V_\|\tau_0(\sigma_x k_y - \sigma_y k_x), \qquad (2)$$

where $C = C_0 + C_\| k_\|^2$, $M = M_0 + M_\| k_\|^2$, and the operator $\boldsymbol{\tau}$ refers now to two decoupled sets of massive Dirac fermions. The last term in Eq. (2) ensures the characteristic *spin-orbital texture* of the TI surface states [44,45].

Figure 2 shows the film-thickness dependence of the parameters of the Hamiltonian (2) for the TIs considered (the plotted values are listed in Tables S2–S4 of the SM [34]). In contrast to the bulk TIs, for all thicknesses the four-band $\mathbf{k}\cdot\mathbf{p}$ spectrum does not have an absolute gap [see the red lines with solid circles in Figs. 1(d)–1(f) for two-QL films and Figs. S2–S4 of the SM [34] for other thicknesses]. Note that only for two QLs and only for Bi_2Te_3 does the eight-band Hamiltonian (blue lines with open rhombuses) provide a quality close to that achieved in the 3D case.

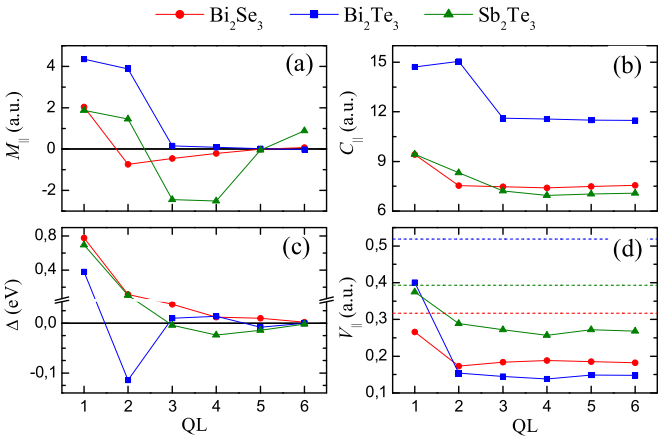

FIG. 2. The parameters of the Hamiltonian (2) for film thicknesses from one QL to six QLs. Here, $\Delta = 2M_0(-1)^{1+\nu_{2D}}$ is the band gap at $\bar{\Gamma}$, with ν_{2D} being the $\mathbb{Z}_2$ topological invariant. The horizontal dashed lines in the $V_\|$ panel show the prediction by the 2D continuous model in the large thickness limit.

Velocity $V_\|$ and electron-hole asymmetry $C_\|$ converge quite fast with the film thickness [Figs. 2(b) and 2(d)], changing only slightly after three QLs. The six-QL value of $V_\|$ can thus be compared with the Fermi velocity from the effective models (see, e.g., Ref. [17]) in the large-thickness limit. In this limit the velocity is expressed in terms of the *bulk* parameters (Table I) as $V_\|\sqrt{1 - C_z^2/M_z^2}$ [shown by the horizontal dashed line in Fig. 2(d)], obviously overestimating the calculated values. The parameter $C_\|$ is positive everywhere, and it is notably larger than the absolute value of the diagonal dispersion term $M_\|$.

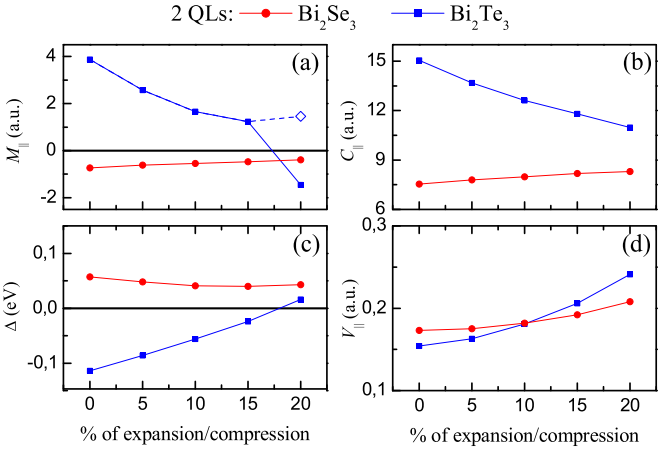

FIG. 3. The parameters of the Hamiltonian (2) for the two-QL film as a function of the van der Waals spacing. The expansion for Bi_2Te_3 and compression for Bi_2Se_3 are given in percents of the bulk values. The dashed blue line in (a) shows the smooth behavior of $|M_\||$.

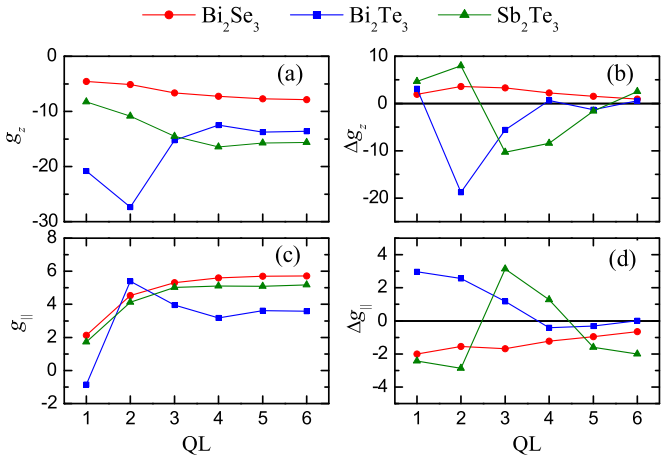

FIG. 4. The effective Landé g factors $g_{z(\|)}$ and $\Delta g_{z(\|)}$ entering the Zeeman term (3) as functions of the film thickness.

For the same thickness, the parameter $M_\|$ may have *different signs* for different TIs, whereas for a given material $M_\|$ is found to "oscillate" with the number of QLs. It turns out that these oscillations do not correlate with the $\mathbb{Z}_2$ topological invariant ν_{2D} obtained from the parities of the original wave functions at the TRIMs of the 2D BZ. This becomes evident from a comparison with the behavior of the gap parameter Δ, whose absolute value $|\Delta| = -2M_0$ yields the gap width at $\bar{\Gamma}$ and the sign depends on ν_{2D}, with Δ being negative for a topologically nontrivial film.

The Sb_2Te_3 film becomes a 2D TI at three QLs and preserves this property up to six QLs [Fig. 2(c)]. For Bi_2Te_3, the two-QL film is nontrivial, then three and four QLs are trivial, and five and six QLs are again nontrivial. The films of Bi_2Se_3 are, on the contrary, trivial for all the thicknesses, while the effective model of Ref. [17] predicts them to be a QSHI at some of the thicknesses. It should also be noted that for the same film the true invariant may depend on details of the crystal geometry and even on the band structure method, including the choice of exchange-correlation potential (see Refs. [46–52]). We emphasize that here the topological invariant and the $\mathbf{k}\cdot\mathbf{p}$ parameters are fully consistent because they are derived from the same band structure.

According to the effective continuous models [17,26], the relation between $C_\|$, M_0, and $M_\|$, one finds in Fig. 2 clearly predicts the absence of edge states. This means that a few-band $\mathbf{k}\cdot\mathbf{p}$ Hamiltonian does not provide a general and certain criterion of the topological character of 2D systems. Because the electron-hole asymmetry term is neglected in the topological analysis [1], it is instructive to consider in more detail the two-QL films of Bi_2Se_3 and Bi_2Te_3—the two thinnest films for which the sign of $M_\|$ correlates with the actual ν_{2D}. In Fig. 3, we see that with varying the van der Waals spacing (expansion for Bi_2Te_3 and compression for Bi_2Se_3) the parameters $V_\|$, $C_\|$, and Δ change steadily, and in Bi_2Te_3 a transition from QSHI to the trivial state occurs (at 18% Δ becomes positive), and at the same time $M_\|$ becomes negative, again following the true indicator ν_{2D}.

Finally, let us consider the effective-mass contribution to the g factor for the films. In our approach, the static magnetic field $\mathbf{B}$ leads to the following Zeeman term,

$$H^{\rm slab}_{\mathbf{kp},Z} = \frac{\mu_B}{2}[g_z\tau_0\sigma_z B_z + g_\|\tau_x(\sigma_x B_x + \sigma_y B_y)] + \frac{\mu_B}{2}[\Delta g_z\tau_z\sigma_0 B_z + \Delta g_\|\tau_y(\sigma_x B_y - \sigma_y B_x)], \quad (3)$$

where $g_\alpha = (g^v_\alpha + g^c_\alpha)/2$ and $\Delta g_\alpha = (g^v_\alpha - g^c_\alpha)/2$.

An interesting feature in Eq. (3) is the second term that contains the z component of the cross product $[\boldsymbol{\sigma}\times\mathbf{B}]$. It is instructive to compare Eq. (3) with the Zeeman term for inversion-asymmetric quantum wells, where the "spin-momentum locking" is also present [4]. As follows from Figs. 4(b) and 4(d), the parameters Δg_z and $\Delta g_\|$ may "oscillate" with the thickness, and for Bi_2Se_3 and Bi_2Te_3 they tend to zero with increasing thickness. As a result, the leading contribution comes from the "conventional term" with g_z and $g_\|$, which at six QLs is already well converged [Figs. 4(a) and 4(c)]. For Sb_2Te_3, Δg_z and especially $\Delta g_\|$ are rather big at six QLs, so the relevant term in $H^{\rm slab}_{\mathbf{kp},Z}$ should be taken into account at least up to this thickness. Note that, in moving from one to six QLs, Δg_z becomes negative for the first time when the film becomes a 2D TI, thus demonstrating a correlation with the topological invariant (see also the effect of expansion/compression for the two-QL films in Fig. S8 of the SM [34]).

To summarize, we have developed a fully *ab initio* $\mathbf{k}\cdot\mathbf{p}$ perturbation approach to generate model Hamiltonians of a desired size. This ensures a physically meaningful behavior of the model Hamiltonian parameters with the continuously varying geometry (van der Waals spacing) and for different numbers of the building layers. By applying our approach to Bi_2Se_3, Bi_2Te_3, and Sb_2Te_3 films, we have demonstrated that the widely used effective continuous models are not able to systematically predict the values and often even the relative sign of the model parameters. The failure to infer the general and certain criterion from $H_{\mathbf{kp}}$ stems from its fundamental limitation: The topological properties of a crystal cannot be unambiguously determined from the behavior of a few bands in the vicinity of $\mathbf{k} = \mathbf{0}$, even though the band inversion occurs just at that point.

This work was supported by the Spanish Ministry of Economy and Competitiveness MINECO (Project No. FIS2013-48286-C2-1-P) and Saint Petersburg State University (Grant No. 15.61.202.2015).

[1] X.-L. Qi and S.-C. Zhang, Topological insulators and superconductors, Rev. Mod. Phys. **83**, 1057 (2011).

[2] H. Weng, R. Yu, X. Hu, X. Dai, and Zh. Fang, Quantum anomalous Hall effect and related topological electronic states, Adv. Phys. **64**, 227 (2015).

[3] H. Zhang, C.-X. Liu, X.-L. Qi, X. Dai, Z. Fang, and S.-C. Zhang, Topological insulators in Bi_2Se_3, Bi_2Te_3, and Sb_2Te_3 with a single Dirac cone on the surface, Nat. Phys. **5**, 438 (2009).

[4] R. Winkler, *Spin-Orbit Coupling Effects in Two-Dimensional Electron and Hole Systems* (Springer, Berlin, 2003).

[5] L. C. Lew Yan Voon and M. Willatzen, *The k. p Method: Electronic Properties of Semiconductors* (Springer, Berlin, 2009).

[6] J. Linder, T. Yokoyama, and A. Sudbø, Anomalous finite size effects on surface states in the topological insulator Bi_2Se_3, Phys. Rev. B **80**, 205401 (2009).

[7] L. Fu and E. Berg, Odd-Parity Topological Superconductors: Theory and Application to $Cu_xBi_2Se_3$, Phys. Rev. Lett. **105**, 097001 (2010).

[8] V. M. Apalkov and T. Chakraborty, Interacting Dirac Fermions on a Topological Insulator in a Magnetic Field, Phys. Rev. Lett. **107**, 186801 (2011).

[9] P. G. Silvestrov, P. W. Brouwer, and E. G. Mishchenko, Spin and charge structure of the surface states in topological insulators, Phys. Rev. B **86**, 075302 (2012).

[10] K. Ebihara, K. Yada, Ai Yamakage, and Y. Tanaka, Finite size effects of the surface states in a lattice model of topological insulator, Physica E **44**, 885 (2012).

[11] Z.-H. Zhu, C. N. Veenstra, S. Zhdanovich, M. P. Schneider, T. Okuda, K. Miyamoto, S.-Y. Zhu, H. Namatame, M. Taniguchi, M. W. Haverkort, I. S. Elfimov, and A. Damascelli, Photoelectron Spin-Polarization Control in the Topological Insulator Bi_2Se_3, Phys. Rev. Lett. **112**, 076802 (2014).

[12] M. Orlita, B. A. Piot, G. Martinez, N. K. S. Kumar, C. Faugeras, M. Potemski, C. Michel, E. M. Hankiewicz, T. Brauner, Č. Drašar, S. Schreyeck, S. Grauer, K. Brunner, C. Gould, C. Brüne, and L. W. Molenkamp, Magneto-Optics of Massive Dirac Fermions in Bulk Bi_2Se_3, Phys. Rev. Lett. **114**, 186401 (2015).

[13] L. Liu, A. Richardella, I. Garate, Yu Zhu, N. Samarth, and C.-T. Chen, Spin-polarized tunneling study of spin-momentum locking in topological insulators, Phys. Rev. B **91**, 235437 (2015).

[14] K. Saha, K. Légaré, and I. Garate, Detecting Band Inversions by Measuring the Environment: Fingerprints of Electronic Band Topology in Bulk Phonon Linewidths, Phys. Rev. Lett. **115**, 176405 (2015).

[15] C.-X. Liu, X.-L. Qi, H. J. Zhang, X. Dai, Z. Fang, and S.-C. Zhang, Model Hamiltonian for topological insulators, Phys. Rev. B **82**, 045122 (2010).

[16] J. C. Slater, Electrons in Perturbed Periodic Lattices, Phys. Rev. **76**, 1592 (1949).

[17] H.-Z. Lu, W.-Y. Shan, W. Yao, Q. Niu, and S.-Q. Shen, Massive Dirac fermions and spin physics in an ultrathin film of topological insulator, Phys. Rev. B **81**, 115407 (2010).

[18] W.-Y. Shan, H.-Z. Lu, and S.-Q. Shen, Effective continuous model for surface states and thin films of three-dimensional topological insulators, New J. Phys. **12**, 043048 (2010).

[19] F. Zhang, C. L. Kane, and E. J. Mele, Surface states of topological insulators, Phys. Rev. B **86**, 081303(R) (2012).

[20] H.-Z. Lu, A. Zhao, and S.-Q. Shen, Quantum Transport in Magnetic Topological Insulator Thin Films, Phys. Rev. Lett. **111**, 146802 (2013).

[21] J. Zhang, C. Triola, and E. Rossi, Proximity Effect in Graphene–Topological-Insulator Heterostructures, Phys. Rev. Lett. **112**, 096802 (2014).

[22] F. Parhizgar, A. G. Moghaddam, and R. Asgari, Optical response and activity of ultrathin films of topological insulators, Phys. Rev. B **92**, 045429 (2015).

[23] S.-B. Zhang, H.-Z. Lu, and S.-Q. Shen, Edge states and integer quantum Hall effect in topological insulator thin films, Sci. Rep. **5**, 13277 (2015).

[24] Y. Zhang, K. He, C.-Z. Chang, C.-L. Song, L.-L. Wang, X. Chen, J.-F. Jia, Z. Fang, X. Dai, W.-Y. Shan, S.-Q. Shen, Q. Niu, X.-L. Qi, S.-C. Zhang, X.-C. Ma, and Q.-K. Xue, Crossover of the three-dimensional topological insulator Bi_2Se_3 to the two-dimensional limit, Nat. Phys. **6**, 584 (2010).

[25] T. Zhang, J. Ha, N. Levy, Y. Kuk, and J. Stroscio, Electric-Field Tuning of the Surface Band Structure of Topological Insulator Sb_2Te_3 Thin Films, Phys. Rev. Lett. **111**, 056803 (2013).

[26] B. Zhou, H.-Z. Lu, R.-L. Chu, S.-Q. Shen, and Q. Niu, Finite Size Effect on Helical Edge States in a Quantum Spin-Hall System, Phys. Rev. Lett. **101**, 246807 (2008).

[27] P. E. Faria, Jr., T. Campos, C. M. O. Bastos, M. Gmitra, J. Fabian, and G. M. Sipahi, Realistic multiband $\mathbf{k}\cdot\mathbf{p}$ approach from *ab initio* and spin-orbit coupling effects of InAs and InP in wurtzite phase, Phys. Rev. B **93**, 235204 (2016).

[28] N. Ray, F. Rost, D. Weckbecker, M. Vogl, S. Sharma, R. Gupta, O. Pankratov, and S. Shallcross, Going beyond $\mathbf{k}\cdot\mathbf{p}$ theory: A general method for obtaining effective Hamiltonians in both high and low symmetry situations, arXiv:1607.00920.

[29] E. E. Krasovskii, Microscopic origin of the relativistic splitting of surface states, Phys. Rev. B **90**, 115434 (2014).

[30] E. E. Krasovskii and W. Schattke, Semirelativistic technique for $\mathbf{k}\cdot\mathbf{p}$ calculations: Optical properties of Pd and Pt, Phys. Rev. B **63**, 235112 (2001).

[31] The extension of the radial basis set provides a high accuracy of the energies and wave functions over a wide energy region from the semicore states to very high energies [see E. E. Krasovskii, Accuracy and convergence properties of the extended linear augmented-plane-wave method, Phys. Rev. B **56**, 12866 (1997)].

[32] E. E. Krasovskii, F. Starrost, and W. Schattke, Augmented Fourier components method for constructing the crystal potential in self-consistent band-structure calculations, Phys. Rev. B **59**, 10504 (1999).

[33] D. D. Koelling and B. N. Harmon, A technique for relativistic spin-polarised calculations, J. Phys. C: Solid State Phys. **10**, 3107 (1977).

[34] See Supplemental Material at http://link.aps.org/supplemental/10.1103/PhysRevB.94.201410 for the bulk TI and related films band structure, the matrix form of model Hamiltonians, the values of Hamiltonian parameters, the analysis of atomic layers maximally contributing to the valence and conduction bands at $\mathbf{k}=\mathbf{0}$, and the effective Landé g factors for two-QL films as a function of the van der Waals spacing.

[35] R. W. G. Wyckoff, *Crystal Structures 2* (Wiley, New York, 1964).

[36] I. A. Nechaev, R. C. Hatch, M. Bianchi, D. Guan, C. Friedrich, I. Aguilera, J. L. Mi, B. B. Iversen, S. Blügel, Ph. Hofmann, and E. V. Chulkov, Evidence for a direct band gap in the topological insulator Bi_2Se_3 from theory and experiment, Phys. Rev. B **87**, 121111(R) (2013).

[37] I. A. Nechaev and E. V. Chulkov, Quasiparticle band gap in the topological insulator Bi_2Te_3, Phys. Rev. B **88**, 165135 (2013).

[38] I. A. Nechaev, I. Aguilera, V. De Renzi, A. di Bona, A. Lodi Rizzini, A. M. Mio, G. Nicotra, A. Politano, S. Scalese, Z. S. Aliev, M. B. Babanly, C. Friedrich, S. Blügel, and E. V. Chulkov, Quasiparticle spectrum and plasmonic excitations

in the topological insulator Sb_2Te_3, Phys. Rev. B **91**, 245123 (2015).

[39] E. E. Krasovskii and W. Schattke, The extended-LAPW-based $\mathbf{k}\cdot\mathbf{p}$ method for complex band structure calculations Solid State Commun. **93**, 775 (1995).

[40] Note that because the basis functions explicitly refer to the valence and conduction band rather than to atomic orbitals. the parameter $M_0 < 0$ that defines the band gap does not change sign upon moving from the topologically nontrivial insulator to the trivial one.

[41] L. Fu and C. L. Kane, Topological insulators with inversion symmetry, Phys. Rev. B **76**, 045302 (2007).

[42] A. Wolos, S. Szyszko, A. Drabinska, M. Kaminska, S. G. Strzelecka, A. Hruban, A. Materna, M. Piersa, J. Borysiuk, K. Sobczak, and M. Konczykowski, *g* factors of conduction electrons and holes in Bi_2Se_3 three-dimensional topological insulator, Phys. Rev. B **93**, 155114 (2016).

[43] B. A. Bernevig, T. L. Hughes, and S.-C. Zhang, Quantum spin Hall effect and topological phase transition in HgTe quantum wells, Science **314**, 1757 (2006)

[44] H. Zhang, C.-X. Liu, and S.-C. Zhang, Spin-Orbital Texture in Topological Insulators, Phys. Rev. Lett. **111**, 066801 (2013).

[45] Y. Cao, J. A. Waugh, X.-W. Zhang, J.-W. Luo, Q. Wang, T. J. Reber, S. K. Mo, Z. Xu, A. Yang, J. Schneeloch, G. D. Gu, M. Brahlek, N. Bansal, S. Oh, A. Zunger, and D. S. Dessau, Mapping the orbital wavefunction of the surface states in three-dimensional topological insulators, Nat. Phys. **9**, 499 (2013).

[46] C.-X. Liu, H. J. Zhang, B. Yan, X.-L. Qi, T. Frauenheim, X. Dai, Z. Fang, and S.-C. Zhang, Oscillatory crossover from two-dimensional to three-dimensional topological insulators, Phys. Rev. B **81**, 041307(R) (2010).

[47] K. Park, J. J. Heremans, V. W. Scarola, and D. Minic, Robustness of Topologically Protected Surface States in Layering of Bi_2Te_3Thin Films, Phys. Rev. Lett. **105**, 186801 (2010).

[48] M. Kim, C. H. Kim, H.-S. Kim, and J. Ihm, Topological quantum phase transitions driven by external electric fields in Sb_2Te_3 thin films, Proc. Natl. Acad. Sci. USA **109**, 671 (2012).

[49] G. Bihlmayer, Yu. M. Koroteev, T. V. Menshchikova, E. V. Chulkov, and S. Blügel, *Ab Initio Calculations of Two-Dimensional Topological Insulators* in *Topological Insulators, Fundamentals and Perspectives* (Wiley-VCH, Weinheim, 2015).

[50] T. Förster, P. Krüger, and M. Rohlfing, Two-dimensional topological phases and electronic spectrum of Bi_2Se_3thin films from *GW* calculations, Phys. Rev. B **92**, 201404(R) (2015).

[51] T. Förster, P. Krüger, and M. Rohlfing, *GW* calculations for Bi_2Te_3 and Sb_2Te_3 thin films: Electronic and topological properties, Phys. Rev. B **93**, 205442 (2016).

[52] T. V. Menshchikova *et al.* (unpublished).